Coupled Seismic and Tracer Test Inversion for Aquifer Property Characterization

STP Volume 3, No. 5
April 1993

David W. Hyndman
Dept. of Applied Earth Sciences

Jerry M. Harris
Dept. of Geophysics

Steven M. Gorelick
Dept. of Applied Earth Sciences

This research was conducted with the support of National Science Foundation Grant BSC-8957186. The computer resources necessary for this project were provided by Hewlett Packard. Seismic inversion software was provided by the Seismic Tomography Project, an Industrial Affiliates program sponsored by the oil and gas industry.

COUPLED SEISMIC AND TRACER TEST INVERSION FOR AQUIFER PROPERTY CHARACTERIZATION

David W. Hyndman
Dept. of Applied Earth Sciences

Jerry M. Harris
Dept. of Geophysics

Steven M. Gorelick
Dept. of Applied Earth Sciences

ABSTRACT

Seismic and tracer test data can contribute valuable information to the estimation of spatial patterns of aquifer hydraulic conductivity. We present the Split Inversion Method (SIM) which combines crosswell seismic and natural gradient tracer test data in a parameter estimation algorithm. First, seismic traveltime tomography estimates the seismic velocity field between two wells, producing a tomogram. The boundaries between large-scale lithologic zones are estimated using the tomogram and the histogram of the estimated seismic velocity values in this field. A simulation-regression procedure simulates groundwater flow and solute transport of a tracer though this estimated lithologic geometry to determine flow and transport parameters. Finally, the lithologic boundaries are refined with a co-inversion of seismic and tracer data. Through iteration, the parameters and boundaries are updated until stable estimates are achieved. The result is a robust identification of the location and shape of large-scale lithologic zones, as well as the mean seismic velocity, hydraulic conductivity, and dispersivity within each zone. The method is demonstrated for a synthetic sandy aquifer with interbedded clay lenses. Results show that inter-well heterogeneities are successfully mapped and accurate hydraulic and seismic parameters are determined.

INTRODUCTION

Groundwater flow, and thus advective transport, is often predominantly controlled by large scale heterogeneity in hydraulic conductivity. Reliable solute transport predictions depend on accurate estimates of such spatially variable aquifer properties. The values of hydraulic properties are typically developed using geostatistical interpolation between a limited number of direct estimates at wells. Unfortunately, any approach using interpolation may result in unrepresentative parameter values.

Geophysical methods provide inexpensive alternatives to invasive drilling programs for aquifer characterization. For example, crosswell seismic tomography provides densely sampled spatial information that complements the spatially averaged information obtained from traditional groundwater methods such as pump tests and tracer tests. Geophysical and hydrogeologic information can be combined to provide a greatly improved description of aquifer properties.

A limited amount of work has focused on combining seismic and hydraulic data to estimate aquifer properties. *Rubin et al.*, [1992] present a method that estimates a two-dimensional hypothetical hydraulic conductivity field given head and hydraulic conductivity measurements at several wells, and perfect knowledge of the seismic velocity field. This method showed that incorporating seismic information can lead to improved hydraulic conductivity estimates. A key assumption is the relation between seismic velocity and hydraulic conductivity. This relationship is complex and may be described, under certain circumstances, by empirical approximations [*Han et al.*, 1986; *Marion et al.*, 1992]. The algorithm of *Rubin et al.* [1992] estimates a pressure field by hydraulic inversion, develops a conductivity field with two possible values for each grid cell using the approximation of *Marion et al.* [1992], and determines the value of hydraulic conductivity at each location that best matches the pressure field from the hydraulic inversion.

We have developed a new parameter estimation algorithm called the Split Inversion Method (SIM). This method combines crosswell seismic tomography and solute tracer test data to estimate the location and shape of large-scale lithologic zones, as well as the effective mean hydraulic conductivity, dispersivity, and seismic velocity of each zone. Based on seismic traveltimes, crosswell tomography is used to estimate the two-dimensional seismic velocity field between wells [*McMechan et al.*, 1987; *Harris*, 1990]. The geometry of lithologic zones is extracted from this velocity field for use in seismic and

tracer simulations. Aquifer parameter values within these zones are estimated using inverse methods of groundwater flow and solute transport simulation [*Wagner and Gorelick*, 1987; *Sun and Yeh*, 1990]. The algorithm iteratively updates the boundaries between zones and the seismic and hydraulic parameters based on feedback from the seismic and tracer test simulations.

The primary assumption in the SIM is that large contrasts in lithology should be manifested as changes in both seismic velocity and hydraulic conductivity. This allows for estimation without a specified relation between seismic and hydraulic parameters. Such a relationship is required to exist, but can be unknown. Thus, in addition to its use as a tool for aquifer parameter estimation, the method may be a useful tool to develop this unspecified parametric relation from field tests. The SIM provides significant advantages over published parameter estimation methods in cases where tracer and crosswell seismic information are available. Parameter uncertainty is reduced by combining two sets of independent data in the estimation procedure. The method is demonstrated with a hypothetical, yet complex, synthetic geologic image.

DEVELOPMENT OF A SYNTHETIC GEOLOGIC IMAGE

We illustrate the method with a hypothetical yet realistic lithologic cross-section. This cross-section represents an inter-well region of a sandy aquifer containing interbedded clay lenses (Figure 1). This common type of lithology could develop in a meandering stream environment or in areas that have experienced marine transgression and regression [*Miall*, 1984]. For example, holocene deposits in the San Francisco Bay area are largely interbedded sands and clays that may fit this conceptual model [*Koltermann and Gorelick*, 1992]. The zonal shapes were designed to test the algorithm's ability to estimate different degrees of lithologic continuity between wells.

The synthetic geologic image was created by placing a model grid over the lithologic structure, and assigning a lithology to each grid cell. A lithologic parameter represents the ratio of sand and clay in the aquifer material which controls the seismic and hydraulic properties. Each grid cell parameter is comprised of two components, a mean value corresponding to sand or clay, and spatially correlated random variability, corresponding to small scale variations that occur in all geologic media. The mean values for saturated sand and clay, shown in Table 1, were taken from text book values [*Freeze*

and Cherry, 1979; *Lankston*, 1990; *McLamore, Anderson, & Espana*, 1978]. The small-scale spatial variability in lithology was represented by a three parameter exponential covariance function {mean = 0.0, variance = 1.0, range = 5.0 meters, no nugget}. The variability was generated by multiplying the Cholesky decomposition [*Golub*, 1989] of this covariance matrix by a vector of standard normal deviates. This produces a random field which closely matches the specified set of correlation statistics [*C. Harvey, personal communication,* 1992].

Two parameter fields were developed based on the former representation of the geologic system: one in terms of hydraulic properties, and the other in terms of seismic properties. First, a hydraulic conductivity field was generated by adding the spatially correlated deviates to the mean natural log hydraulic conductivity values (Figure 1a). This assumes that for each lithologic type, hydraulic conductivity is a second-order stationary log-normally distributed random variable [*Freeze*, 1975; *Hoeksema and Kitanidis*, 1985]. Second, a seismic velocity field was developed by adding a field of deviates with a small variance to the mean seismic velocity values (Figure 1b). A smaller variance is appropriate because the range of seismic velocity in porous media is several orders of magnitude smaller than the range in hydraulic conductivity. We adopted a lognormal model of the small scale variability in seismic velocity. Although this is reasonable, it has not been fully resolved in the geophysics literature. The variance of the seismic velocity deviates was scaled in relation to the range in mean parameter values using:

$$\sigma^2_{\ln(V)\text{ deviates}} = \sigma^2_{\ln(K)\text{ deviates}} \left(\frac{\ln \overline{V}_{sand} - \ln \overline{V}_{clay}}{\ln \overline{K}_{sand} - \ln \overline{K}_{clay}} \right)^2 \qquad (1)$$

where $\overline{V}$ mean seismic velocity, in m/s;

$\overline{K}$ mean hydraulic conductivity, in m/s.

Thus, approximately four orders of magnitude less variability was added to the log seismic velocity field than to the log hydraulic conductivity field.

Two synthetic data sets, seismic traveltimes and tracer concentrations, were developed by simulating the physics of solute transport and sound wave propagation through these parameter fields (Figure 2). Such data sets are easily collected in the field. We assume our synthetic values represent measurements from field tests conducted with

limited resources. Seismic field methods can be designed to gather more information about subsurface heterogeneity than provided by the simulated tests in this study, but such methods are much more difficult and expensive to use.

SEISMIC TRAVELTIME GENERATION

In field studies, measured data for seismic velocity inversions are the times for seismic waves to travel from source to receiver locations. For a crosswell test, a seismic source is activated by generating sound waves at specified depth intervals in one well, while hydrophones or geophones measure the propagated wave field at multiple depths in nearby wells. The received wavefield is analyzed for key events, such as the compressional wave arrival time at each receiver [*Telford et al.*, 1990]. Although not used here, other key wavefield events include shear wave arrival times and reflection arrival times from lithologic interfaces.

Compressional wave traveltimes are simulated using a code that integrates the traveltimes from source positions to receiver positions along discrete paths through the seismic velocity field. These discrete paths, or rays, bend in heterogeneous media because seismic energy is refracted as described by Snell's Law [*Telford et al.*, 1990].

$$\frac{(\sin \theta_1)}{v_1} = \frac{(\sin \theta_2)}{v_2} = \frac{(\sin \theta_i)}{v_i} = \frac{(\sin \theta_n)}{v_n} \qquad (2)$$

where q_i angle between the ray in zone i and the normal to an interface separating zone i from zone i+1

V_i seismic velocity in zone i

The synthetic seismic traveltimes were generated to represent measured field data. To avoid using the same ray tracing algorithm as is used in the inversion, traveltimes were generated using the following steps:

1) Traveltimes were simulated for large scale constant velocity zones using a sharp interface ray tracing algorithm originally developed by *Cerveny* [1985] then modified for the crosswell geometry [*S. Lazaratos, personal communication,* 1992]. These constant

velocity zones are separated by sharp boundaries and assigned the mean values listed in Table 1. Each ray is linked from a source position to a receiver position by simulating rays with different initiation angles until the ray reaches the well near a specified receiver location.

2) Traveltimes were again simulated through a gridded version of the image with constant velocity zones using the initial-value scheme of [*Harris*, 1992].

3) Traveltimes were then simulated through a gridded velocity image with added correlated variability. Figure 2a shows a subset of the simulated raypaths from one source through this heterogeneous seismic velocity field.

4) The difference between the traveltimes simulated in step 2 and step 3 represents the effect of the correlated velocity variability on the traveltimes. This difference was added to the traveltimes from step 1 to make up our measured seismic data set.

SYNTHETIC CONCENTRATION DATA

Along with seismic traveltime data, our method requires solute tracer test data. This data was developed by simulating a natural hydraulic gradient (1%) tracer test from a slug input of solute to a well through the synthetic aquifer shown in Figure 1a. The concentrations at the down-gradient well were vertically flux averaged [*Parker and Van Genuchten*, 1984] assuming the well was fully screened and that multiport sampling was not available. The flux averaged concentration was calculated as the sum of each well grid cell concentration times the specific discharge in this cell divided by the total specific discharge into the well. Multiport sampling would allow significantly better spatial resolution of aquifer heterogeneity, but is seldom used in the field. The two wells are assumed to be in a plane parallel to the regional hydraulic gradient and the lithology is assumed to be horizontally continuous in a direction perpendicular to this gradient. Flow and dispersion in and out of this plane is neglected for simplification. Future work is aimed toward a full three-dimensional representation of aquifer heterogeneity.

The concentration history provides information about the nature of aquifer heterogeneity. The small scale dispersivity and the variability of hydraulic conductivity are responsible for the gross apparent spreading in the concentration history. Figures 2b and

2c show dispersion of the tracer plume during its migration from the source well to the down-gradient well. These images indicate the nature of tracer transport in this type of environment. Such spatial information between wells is assumed to be unavailable and therefore is not used in the inversion. The low solute concentrations in the clay through time verify that these zones represent effective barriers to flow. As long as the clay zones have a hydraulic conductivity several orders of magnitude lower than the sand zones, the simulated concentration history was found to be insensitive to the hydraulic conductivity and dispersivity of the clay. The hydraulic conductivity and dispersivity of the clay are thus fixed (see Table 2) throughout the estimation procedure.

SEISMIC INVERSION: CROSSWELL SEISMIC TOMOGRAPHY

Crosswell seismic tomography is similar to the Computer Aided Tomography (CAT) scan developed for medical imaging [*Dines and Lytle*, 1979]. Compressional-wave traveltimes for each source-receiver pair are used as data in an iterative seismic inversion which estimates the seismic velocity field between two wells. The seismic velocity in each pixel of a grid is obtained by iteratively tracing rays through a velocity field and projecting portions of the difference between simulated and observed (residual) traveltimes along these estimated ray paths [*Harris*, 1990]. This iterative nonlinear inversion has two sets of unknowns, the seismic velocity in every pixel and the ray paths between each source and receiver. The equations approximated in this code involve integration of the velocity along a ray path to give a predicted traveltime:

$$t_i = \int_{C_i} S(x,z)\, dl \qquad (3)$$

where

t_i	traveltime for ray (i), {s};
$S(x,z)$	= 1 / V(x,z), seismic slowness, {s/m};
$V(x,z)$	seismic velocity, {m/s};
l	path length along the contour of a ray, {m}.

Equation (3) can be linearized by separating perturbations (δS) from a background slowness field (S_0):

$$S(x,z) = S_0(x,z) + \delta S(x,z) \text{ with pertubations:} \quad (4a)$$

$$\delta S(x,z) = \sum_{j}^{N} \beta_j \psi_j(x,z) \quad (4b)$$

Using the small perturbation approach described in (4a) and (4b), the inversion reduces to a linear system of equations:

$$\delta t = W \beta \text{ where the elements of W are: } W_{i,j} = \int_{C_i} \psi_j(x,z)\, dl \quad (5)$$

where:

δt	array of residual traveltimes;
$\psi_j(x,z)$	basis function for the perturbation expansion;
W	projection matrix with terms being the ray path lengths in the pixels when the basis function $\psi_j(x,z)$ is chosen to be a rectangular pixel;
β	array of unknown coefficients describing the average slowness perturbation along individual ray paths.

The projection matrix (W) is sparse because each ray intersects a small fraction of the total pixels. This results in a large system of equations (5) which cannot be easily inverted in closed form. The matrix system (5) is thus solved using a Simultaneous Iterative Reconstruction Technique (SIRT) [*McMechan et al.*, 1987] where a portion of the residuals from multiple (N) rays are simultaneously superposed to determine the resulting slowness change for each pixel. Other inversion algorithms, such as conjugate gradients, can also be used to invert (5).

Tomographic traveltime inversion using SIRT is a robust seismic velocity estimation technique [*Dines and Lytle*, 1979; *McMechan et al.*, 1987; *Harris*, 1990]. Because this is an iterative method, an initial estimate of the velocity field is needed to determine raypaths. For this simulation, the constant seismic velocity field that best fits the traveltime data for straight ray paths was initially used. In a field test, a better estimate of this initial field can be created from seismic velocity logs taken in the source and receiver wells. The ray tracing algorithm traces fans of rays from the source well through this constant velocity field to the receiver well where each ray termination is interpolated to the nearest receiver. Part of the residual between the simulated and measured traveltime for each ray is then distributed along the estimated ray path in a process called backprojection.

Because the ray paths are unknown, the backprojection of the entire residual along estimated ray paths would result in significant errors in the estimated seismic velocity. The velocity changes due to individual backprojections are thus damped to retain the small perturbation approximation described by (4) and (5). In repeated iterations, rays are traced through updated velocity images throughout which residuals are again distributed. This iterative procedure continues until the traveltime residuals are small. The result is convergence toward a relatively smooth velocity image, called a tomogram, which in our case exhibits the large scale structure (Figure 3a) of the synthetic aquifer (Figure 3g).

SPLIT INVERSION METHOD (SIM) WITH SEISMIC DATA

For this work, we have developed the Split Inversion Method (SIM) method which extracts useful information from crosswell seismic tomograms for hydrogeologic analysis. This method identifies large scale lithologic zones with high resolution and estimates effective seismic velocities for these zones. Using SIM, traveltime tomography accurately identifies the general locations and shapes of zones with different lithology.

The seismic field estimated from tomography alone contains artifacts due to residuals being backpropagated into regions with few ray intersections. These artifacts are seen as streaks through the tomogram in Figure 3a. To reduce the effect of these artifacts and retain the large scale structure, we smooth the tomogram using a weighted averaging procedure called Hanning [*Tukey*, 1977; *Velleman and Hoaglin*, 1981] resulting in the tomogram in Figure 3b. We then generate a histogram of seismic velocity values in this smoothed tomogram (Figure 4b). This statistical distribution of seismic velocity values shows a clear signature of lithologic properties and provides a basis for extracting the large-scale features of the estimated seismic velocity field. In the example case, the histogram shows a bimodal distribution. The dominant peak corresponds to sand and the smaller peak indicates the presence of low velocity clay zones.

The SIM separates the tomogram into lithologic zones using the statistical information from the histogram and the spatial information from the tomogram. Recall that the simulated seismic traveltimes through the zonal image depend on the lithologic zonation. This zonation is adjusted by changing the value of seismic velocity that separates different zones. That is, these traveltimes depend on the seismic velocity that delineates the boundaries of the homogeneous zones. This method thus adjusts the boundaries until the

minimum seismic traveltime residuals are obtained. An efficient bisection method called the golden search strategy [*Press et al.*, 1989] is used for this minimization. For each evaluated boundary velocity, a constant seismic velocity value is assigned to each zone based on the histogram. For the high velocity zones, which represent sand in our case, we assigned the mode of estimated velocities because the mode is a good estimate of the central property of the bulk matrix material. For the low velocity zones, which represent clay in our case, we assigned the lowest seismic velocity from the smoothed tomogram.

The lowest smoothed velocity was chosen to represent the clay zones because few extreme values within these small zones are estimated due to the damping imposed by the seismic traveltime inversion. This poor estimation of extremes can be seen in the histogram of the smoothed seismic velocity field in Figure 4b as compared to the histogram of the synthetic velocity field in Figure 4a. The clay mode centered at approximately 1520 m/s in Figure 4a is poorly represented in Figure 4b. Backprojection of residuals along entire ray paths led to a relatively smooth estimated velocity field with few extreme values (Figure 3a). Any remaining small scale variability was removed when the tomogram was smoothed (Figure 3b), thus the minimum smoothed velocity is a reasonable estimate of the mean clay velocity. Other estimates of this seismic velocity, such as the median and mode of the low velocity values, consistently underestimate the synthetic mean value.

The SIM produces a tomogram (Figure 3c) with accurate estimates of the location and geometry of lithologic zones in the synthetic shown in Figure 3g, with the exception of a small extraneous zone near the upper portion of the down gradient well. The mean values of seismic velocity estimated for these zones are very close to the synthetic mean values (Table 2). The lithologic zones determined from the seismic inversion method (SIM) are also used in a tracer test inversion which estimates flow and transport parameters. This procedure is discussed in the next section.

TRACER TEST INVERSION

Hydraulic conductivity and dispersivity values for the sand zones delineated from the SIM are estimated using a simulation-regression procedure [*Wagner and Gorelick*, 1987; *Gailey et al.*, 1991]. This methodology combines solute transport simulation (SUTRA, [*Voss*, 1984]) with weighted nonlinear least squares regression analysis (STARPAC, [*Donaldson and Tryon*, 1990]). Our formulation involves minimizing the

difference between simulated and observed concentrations, and simulated and observed peak concentration arrival time.

$$\text{Minimize} \sum_{T=0}^{T'} \{(C_{T,meas} - C_{T,sim})^2\} + \lambda (t_{p,\,meas} - t_{p,\,sim})^2 \qquad (6)$$

where

$C_{T,meas}$	measured concentration at down-gradient well at time T, {mg/L};
$C_{T,sim}$	simulated concentration at down-gradient well at time T, {mg/L};
$t_{p,\,meas}$	measured time of peak concentration arrival, {hours};
$t_{p,\,sim}$	simulated time of peak concentration arrival, {hours};
T	time increment since slug input of tracer at up-gradient well, {hours};
T'	time at which breakthrough is complete, {hours};
λ	weighting factor, $\{mg^2/(L^2 \cdot hours^2)\}$.

We simulate steady groundwater flow and nonreactive solute transport through a heterogeneous aquifer using:

The groundwater flow equation,

$$\nabla \cdot (\mathbf{K} \nabla h) = 0 \qquad (7)$$

Darcy's Law,

$$v = -\frac{\mathbf{K}}{\theta} \nabla h \qquad (8)$$

and the advection dispersion equation.

$$\theta \frac{\partial c}{\partial t} + \theta\, v \cdot \nabla c - \theta \nabla \cdot (\mathbf{D} \nabla c) = 0 \qquad (9)$$

where

—	gradient operator, $(\partial/\partial x, \partial/\partial z)$;
x, z	Cartesian coordinates, {m};
K	hydraulic conductivity tensor, {m/s};
h	hydraulic head, {m};
v	groundwater velocity, {m/s};
q	effective porosity, {dimensionless};

c	concentration of conservative tracer, {mg/L^3};
t	time, {s};
D	**D** = **D**(α_L,v), hydrodynamic dispersion tensor, {m^2/s};
α_L	longitudinal dispersivity, {m}.

The estimated flow and transport parameters are listed in Table 2. Despite small-scale variability in hydraulic conductivity, the conductivity estimate is very close to the mean synthetic value. The large scale estimated sand dispersivity, α_L = 3.29 meters, is large compared to the synthetic small scale value, α_L = 1.0 meters. This difference is expected because the large scale estimate of dispersivity accounts for velocity variations at all scales smaller than the lithologic zones which are presumed to be homogeneous in the transport model. The estimated dispersivity is thus an effective parameter for the lithologic zones, and its general magnitude is consistent with stochastic transport theory [*Gelhar and Axness*, 1983]. The theory says that the asymptotic longitudinal dispersivity should be approximately:

$$\alpha_L \approx \sigma^2 \lambda/\gamma^2 \qquad (10)$$

where	σ^2	the variance of ln(K);
	λ	the correlation length;
	γ	a flow factor, $\gamma \approx 1+\sigma^2/6$ for isotropic cases.

Other authors, such as [*Neuman et al.*, 1987], suggest that use of this flow factor is inappropriate and should be neglected. This asymptotic value would theoretically be reached after the solute has adequately sampled all scales of variability (after 40 to 50 correlation lengths according to *Dagan* [1982]). These stochastic theories indicate that the asymptotic longitudinal dispersivity would be in the range of 3.7 - 5.0 meters, which is expectedly larger but in the general range of our pre-asymptotic value of 3.3 meters.

The least squares fit between the simulated and observed concentration histories is shown in Figure 5. The best fit is near the peak since the formulation specified in (6) gives extra weight to the time of peak concentration arrival. The time of peak concentration arrival is highly sensitive to the hydraulic conductivity value and thus provides a strong control on the estimated parameter values. Without matching to the peak arrival time, the algorithm was found to be insensitive to hydraulic conductivity when this

estimated value is several orders of magnitude larger than the synthetic value. This would only occur with a poor initial guess of the hydraulic conductivity. This insensitivity arises when the estimated hydraulic conductivity is large enough to allow transport of the entire tracer plume through the media before the field plume arrived, and thus the concentration histories would not overlap.

In our procedure, we placed a lower bound on the estimated dispersivity values. Penalty weights were placed on dispersivity for values outside of the range of numerical accuracy. Numerical dispersion and oscillations were found to cause significant problems in this type of estimation algorithm because a discontinuity would arise in the gradient of the objective function (6) in these parameter ranges. In our case, dispersivity was restricted to values greater than 0.25 m to ensure concurrence with the Peclet criteria of $\frac{\Delta x}{\alpha} \leq 4$. [*Voss*, 1984] where Δx is the grid spacing (1 m in this case).

SPLIT INVERSION METHOD (SIM) WITH TRACER AND SEISMIC DATA

Independent inversions based on the seismic and tracer data provide a reasonable first cut representation of the lithology. As discussed earlier, the SIM with seismic data alone estimates the shape of large-scale lithologic zones and the seismic velocity within these zones. The tracer test inversion then provides initial flow and transport parameter estimates for these zones (Table 2). The flowchart in Figure 6 shows where these initial estimates fit into the overall parameter estimation algorithm.

An updated estimate of the seismic velocity field is obtained using seismic tomography with the binary tomogram from SIM (Figure 3c) as the initial velocity estimate. The resulting tomogram (Figure 3d) has better estimates of the clay velocity and fewer artifacts than the earlier tomogram (Figure 3a). The histogram of this estimated velocity field (Figure 4c) shows the sand and clay distributions of Figure 4a much better than the previous histogram (Figure 4b). The small scale heterogeneity was more accurately estimated in Figure 3d because the initial seismic velocity field for this inversion was much closer to the synthetic image. The smoothed version of this tomogram (Figure 3e) retained the large-scale structure with significantly less artifacts than the tomogram in Figure 3b.

The SIM can produce better results if the two inversions are combined in a procedure which uses both data sets concurrently. This final step of the algorithm determines the zonation which best satisfies both the seismic and tracer data using the tomogram in Figure 3e and a histogram of the seismic velocity values in this tomogram (Figure 4c). This gave an improved representation of the large scale lithology in the synthetic aquifer (Figure 3g). All the clay zones were properly identified and the mean seismic velocities within the sand and clay zones were accurately estimated (Table 2). No extraneous zones were present in this binary image.

The SIM described in the earlier section, Split Inversion Method with seismic data, is used again with the exception that both concentration and traveltime residuals are now considered. The sum of residuals between simulated and observed seismic traveltime, tracer concentrations, and peak concentration arrival time is minimized. As shown in Figure 7, the minimum seismic residuals and the minimum tracer concentration residuals are at similar values of seismic split velocity. This indicates that the zones are relatively consistent with both sets of information. The minimum concentration residuals occur at a slightly larger value of seismic split velocity than the minimum seismic residuals. Thus for this synthetic test, the best zonation for the tracer data contains slightly larger clay zones than indicated by the seismic data. This gives a more accurate estimate of the lithologic geometry than would be obtained with seismic data alone. A final tracer inversion is then performed using the new zonation to obtain flow and transport parameter estimates for the updated boundaries. The updated boundaries changed by a minor amount, therefore the tracer parameter estimates did not change significantly. If the boundaries and parameter estimates are stable with minima at similar seismic split velocities, the inversion is complete. If there are still significant changes in the boundaries, this procedure iteratively updates the zonation and the zoned parameter estimates. The SIM with two independent data sets results in refined zonation and parameter estimates which are consistent with the physical processes that relate to these data.

CONCLUSION

This research demonstrates that geophysical and hydrogeologic data can be coupled to identify the location and shape of large-scale lithologic zones, and to estimate the mean seismic velocity, hydraulic conductivity and dispersivity within these zones. Crosswell seismic tomography provides densely sampled information about lithologic heterogeneity, supplementing the spatially averaged information from the inversion of tracer test data. The seismic traveltime data are sensitive to the geometry of lithologic zones and the seismic velocity within these zones. An initial seismic inversion gives an estimated seismic velocity field. The Split Inversion Method (SIM) effectively extracts the large scale lithologic structure from this estimated seismic velocity field by distinguishing between sand and clay zones. Flow and transport parameters are then estimated for the determined lithologic zones using a simulation-regression procedure. The nonreactive tracer concentration data are sensitive to the geometry of lithologic zones and the hydraulic conductivity and dispersivity within these zones. A final combined inversion using the SIM with both seismic and tracer data refines the lithologic boundaries and parameter estimates. This methodology is robust because it provides estimates which are consistent with two independent data sets.

The methodology developed here is directed toward future application with field data. First, extensions of this work could utilize readily available seismic data. Although we have used only traveltime measurements as the seismic data, we have been able to identify lithologic patterns between wells. In a field test, the full seismic wave field is measured and the seismic velocity structure near the wells is estimated using well logs. Modeling the full wave field or multiple wave attributes may offer significantly more information about aquifer lithology than provided by traveltimes alone. Lithologic estimates can also be improved by conditioning on local well log information. Second, seismic wavelength can be adjusted to obtain lithologic information at different scales. Seismic waves measure the average seismic velocity across the Fresnel zone. The width of this zone in a direction perpendicular to ray paths is directly related to the wavelength of the seismic energy. The attenuation of the energy, however, is inversely related to wavelength. This results in a tradeoff between small wavelength energy that produces very high resolution but can only be used for closely spaced wells, and longer wavelength energy that produces less resolution but can be used for wells spaced at larger distances. For closely spaced wells, seismic tests over a range of wavelengths would produce data to resolve heterogeneity at different scales.

The methodology could also be extended to three-dimensions. In such a case, an ideal field tracer test design consists of a recharge well, which would inject water and tracer, in the center of a group of pumping wells with multiple sampling zones at different depths. Because this type of test provides three-dimensional information about groundwater flow and solute transport, it would produce much more information about the shape, location, and properties of lithologic zones than produced with a natural gradient tracer test. At contaminated sites where tracer tests can not be implemented, measured contaminant concentrations at various locations through time could serve as a data set.

Other measured information could be used in our parameter estimation algorithm. This information could include pressure response at observation wells due to an applied stress at a pumping or recharge well. Hydraulic information could be especially useful if repetitive seismic tests are completed during a pump test. Different lithologic zones should have different pressure responses that could be monitored by analyzing the changes in seismic velocity through time. As hydraulic pressure decreases, seismic velocity in a porous media increases because of the increased grain to grain stress. The time for a pressure pulse to dissipate is related to the hydraulic conductivity of the media, thus a pressure difference should be observed between high and low conductivity zones. This transient pressure response information should result in accurate parameter estimates and greatly improved knowledge of the relation between seismic velocity, hydraulic pressure, and hydraulic conductivity.

ACKNOWLEDGMENTS

This research was conducted with the support of National Science Foundation Grant BSC-8957186. The computer resources necessary for this project were provided by Hewlett Packard.

REFERENCES

Cerveny, V., The application of ray tracing to the propagation of shear waves in complex media, in *Handbook of Geophysical Exploration*, K. Helbig and S. Treitel ed., 15A, 1-124, Geophysical Press, London, 1985.

Dagan, G., Stochastic transport in heterogeneous porous formations, *J. Fluid Mech.*, 145, 151-177, 1982.

Dines, K. A., and R. J. Lytle, Computerized geophysical tomography, paper presented at IEEE, 1979.

Donaldson, J. R., and P. V. Tryon, Nonlinear least squares regression using STARPAC: The Standards Time Series and Regression Package, Tech. Note 1068-3, Nat. Bur. Stand., Boulder, CO, 1990.

Freeze, R. A., A stochastic-conceptual analysis of one-dimensional flow in nonuniform homogeneous media, *Water Resour. Res.*, 11(5), 725-741, 1975.

Freeze, R. A., and J. A. Cherry, *Groundwater*, Prentice-Hall, Englewood Cliffs, N. J., 1979.

Gailey, R. M., S. M. Gorelick, and A. S. Crowe, Coupled process parameter estimation and prediction uncertainty using hydraulic head and concentration data, *Adv. Water Resour.*, 14(5), 301-314, 1991.

Gelhar, L. W., and C. L. Axness, Three dimensional stochastic analysis on macrodispersion in aquifers, *Water Resour. Res.*, 19(1), 161-180, 1983.

Golub, G. H., *Matrix Computations*, John Hopkins University Press, Baltimore, 1989.

Han, D., A. Nur, and D. Morgan, Effect of porosity and clay content on wave velocity in sandstones, *Geophys*, 51, 2093-2107, 1986.

Harris, J. M., Tomographic string inversion, Expanded Abstracts of the SEG Meeting, p. 84, 1990.

Harris, J. M., Initial value raytracing in smoothly varying heterogeneous media, in *Seismic Tomography Project Report*,, I1-I14, Stanford University, Stanford, CA, 1992.

Hoeksema, R. J., and P. K. Kitanidis, Analysis of the spatial structure of properties of selected aquifers, *Water Resour. Res.*, 21(4), 563-572, 1985.

Koltermann, C. E., and S. M. Gorelick, Paleoclimatic signature in terrestrial flood deposits, *Science*, 256, 1775-1782, 1992.

Lankston, R. W., High-resolution refraction seismic data acquisition and interpretation, in *Geotechnical and Environmental Geophysics*, S. H. Ward ed., 45-72, Society of Exploration Geophysicists, Tulsa, Okla., 1990.

Marion, D. P., A. Nur, H. Yin, and D. Han, Compressional velocity and porosity in sand-clay mixtures., *Geophys.*, 57, 554-563, 1992.

McLamore, V. R., D. G. Anderson, and C. Espana, Crosshole testing using explosive and mechanical energy sources, in *Dynamic Geotechnical Testing*, ed., American Society for Testing of Materials, STP 654, 30-55, Philadelphia, 1978.

McMechan, G. A., J. M. Harris, and L. M. Anderson, Cross-hole tomography for strongly variable media with applications to scale model data, *BSSA*, 77(6), 1945-1960, 1987.

Miall, A. D., *Principles of Sedimentary Basin Analysis*, Springer-Verlag, Heidelberg, Germany, 1984.

Neuman, S. P., C. L. Winter, and C. M. Newman, Stochastic theory of field-scale fickian dispersion in anisotropic porous media, *Water Resour. Res.*, 23(3), 453-466, 1987.

Parker, J. C., and M. T. Van Genuchten, Flux-averaged and volume averaged concentrations in continuum approaches to solute transport, *Water Resour. Res.*, 20(7), 866-872, 1984.

Press, W. H., B. P. Flannery, S. A. Teukolsky, and W. T. Vetterling, *Numerical Recipes - The Art of Scientific Computing*, Cambridge University Press, Cambridge, 1989.

Rubin, J., G. Mavko, and J. Harris, Mapping permeability in heterogeneous aquifers using hydrologic and seismic data, *Water Resour. Res.*, 28(7), 1809-1816, 1992.

Sun, N.-Z., and W. W.-G. Yeh, Coupled inverse problems in groundwater modeling 1. Sensitivity analysis and parameter estimation, *Water Resour. Res.*, 26(10), 2507-2525, 1990.

Telford, W. M., L. P. Geldart, and R. E. Sheriff, *Applied Geophysics*, Cambridge University Press, Cambridge, 1990.

Tukey, J. W., *Exploratory Data Analysis*, Addison-Wesley Publishing Company, Reading, Mass., 1977.

Velleman, P. F., and D. C. Hoaglin, *Applications, Basics, and Computing of Exploratory Data Analysis*, Wadsworth, Inc., Belmont, 1981.

Voss, C. I., Saturated-Unsaturated Transport (SUTRA): A finite-element simulation model for saturated-unsaturated, fluid-density-dependent ground-water flow with energy transport or chemically-reactive single-species solute transport, U. S. Geol. Surv. Water Resour Invest. Rep., 84-4369, 1984.

Wagner, B. J., and S. M. Gorelick, Optimal groundwater quality management under parameter uncertainty, *Water Resour. Res.*, 23(7), 1162-1174, 1987.

Table 1 - Mean parameters in the synthetic model

	sand	clay
Hydraulic conductivity , K (m/s)	10^{-4}	10^{-9}
Effective porosity, q	0.250	0.250
Longitudinal dispersivity, a_L (m)	1.0	1.0
Transverse dispersivity, a_T (m)	0.5	0.5
Seismic velocity (m/s)	1830.	1520.

Table 2 - Parameter estimates relative to the mean values in the synthetic model

Parameter	Estimate	Mean synthetic value
Hydraulic conductivity (sand), {m/s}	$10^{-4.087}$	$10^{-4.0}$
Longitudinal dispersivity (sand), {m}	3.29	1.0

Split #	1	2
Seismic velocity (sand), {m/s}	1800. / 1818.	1830.
Seismic velocity (clay), {m/s}	1571. / 1520.	1520.

Split 1 - initial binary split with seismic information

Split 2 - second binary split with seismic and tracer information

Fixed parameter	Fixed value	Mean synthetic value
Hydraulic conductivity (clay), {m/s}	$10^{-10.4}$	10^{-9}
Longitudinal dispersivity (clay), {m}	2.0	1.0

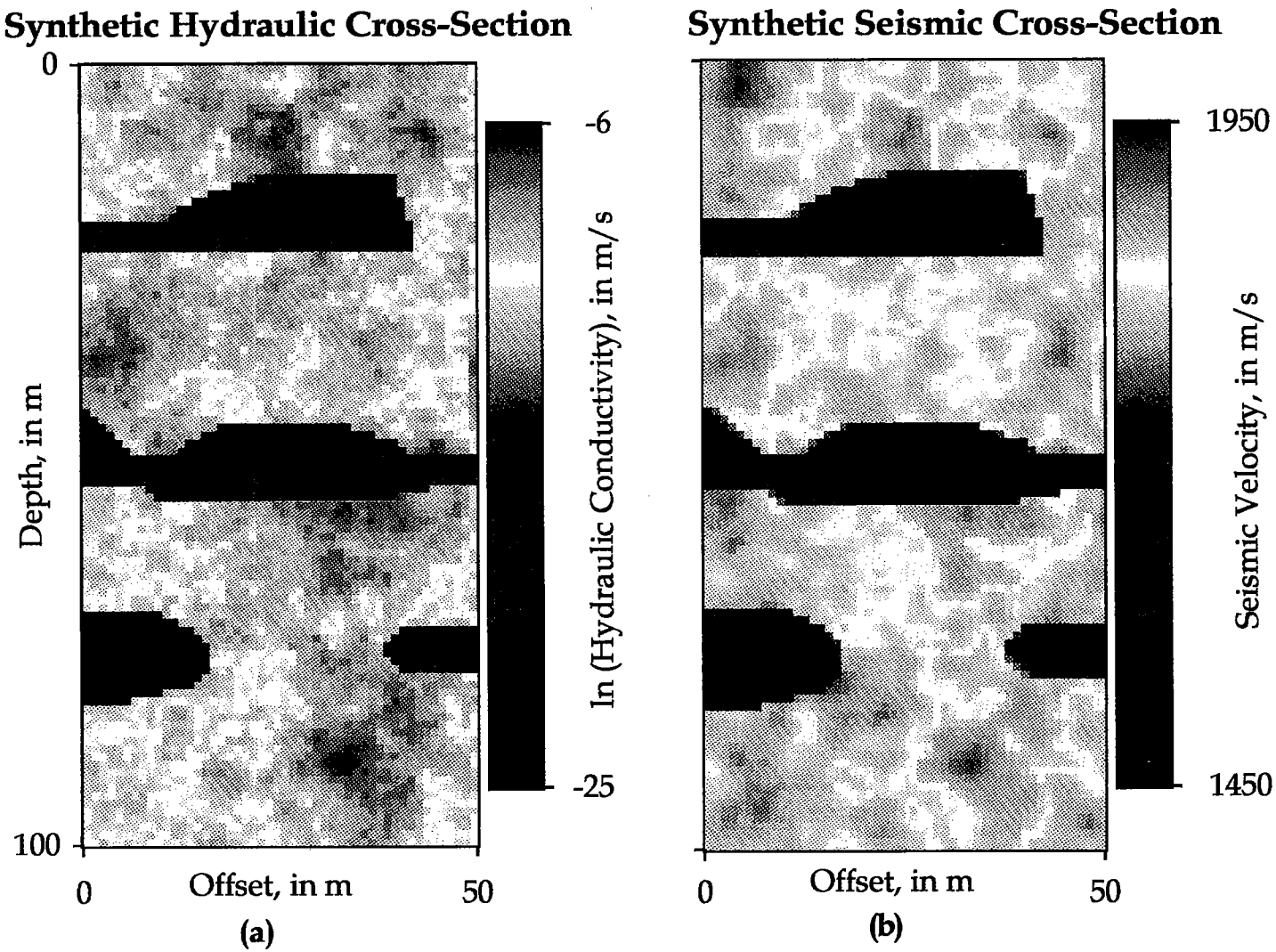

Figure 1. (a) Synthetic hydraulic conductivity field and (b) seismic velocity field used for development of the synthetic data.

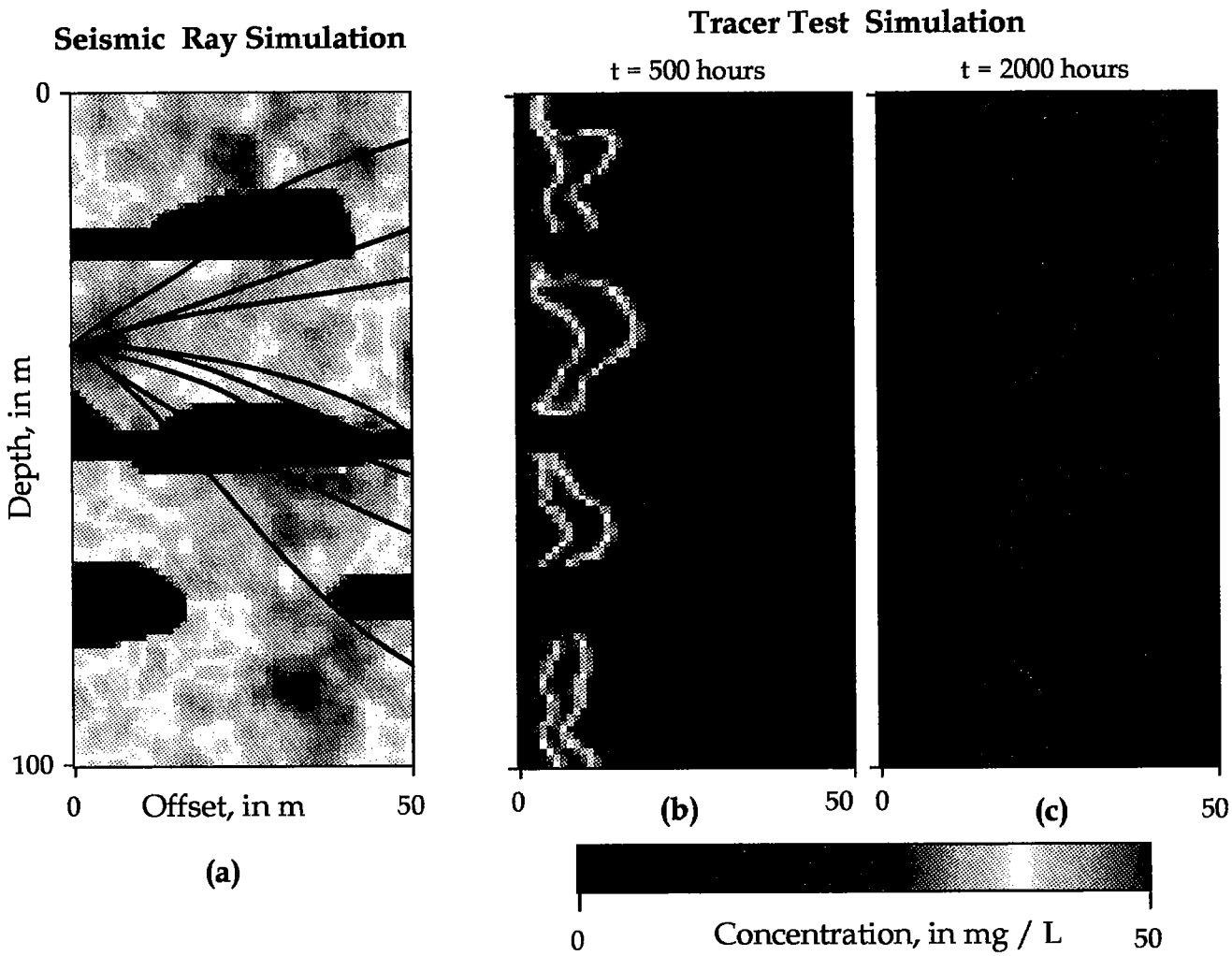

Figure 2. Seismic and tracer test simulations for develpment of synthetic data sets. Seismic rays are traced through the synthetic image in **(a)** and the tracer concentrations are shown at 500 hours **(b)** and 2000 hours **(c)** after the tracer injection for this natural gradient test.

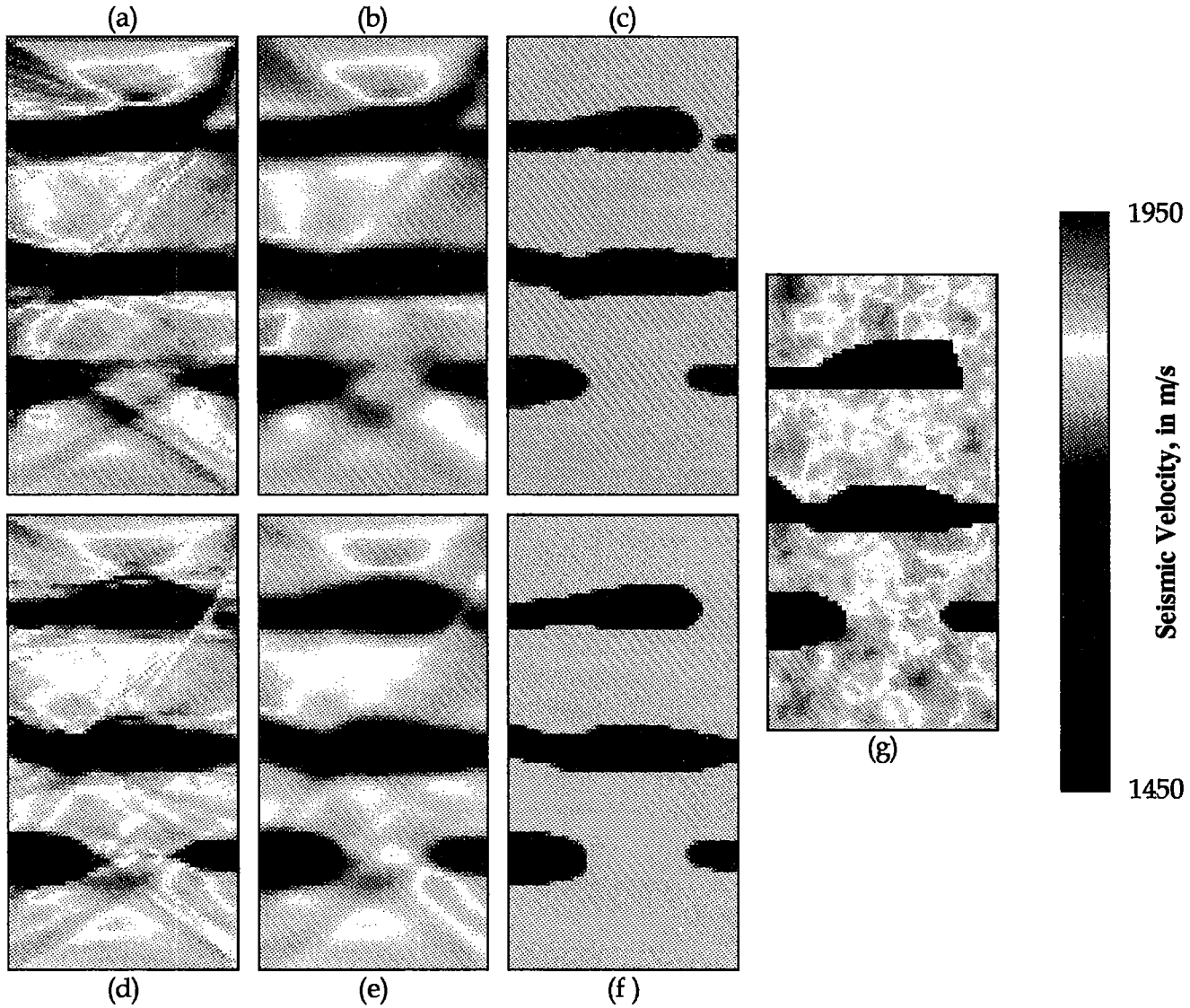

Figure 3. Seismic tomograms after stages of the parameter estimation algorithm. These stages are: (a) Preliminary seismic inversion with constant velocity starting image, (b) Hanning smooth of (a), (c) Split Inversion Method (SIM) with seismic data, (d) Seismic inversion with (c) as starting estimate, (e) Hanning smooth of (d), (f) SIM with tracer and seismic data. These tomograms can be compared with the synthetic seismic velocity field in (g).

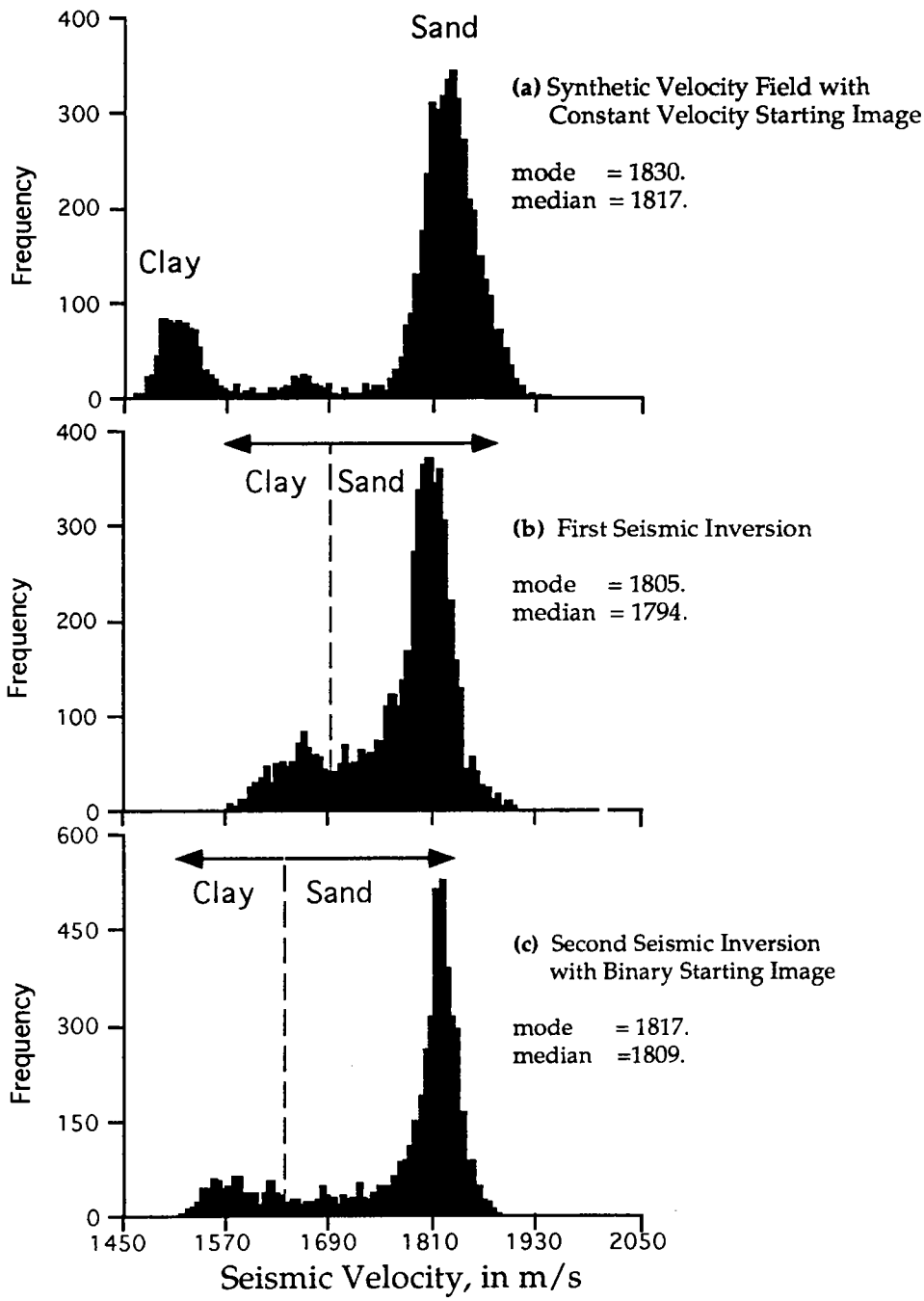

Figure 4. Histograms of seismic velocity in: (a) The synthetic seismic velocity field (Figure 3g), (b) The smoothed seismic velocity field after the first seismic inversion (Figure 3b), (c) The smoothed seismic velocity field from the seismic inversion with a binary starting model (Figure 3e).

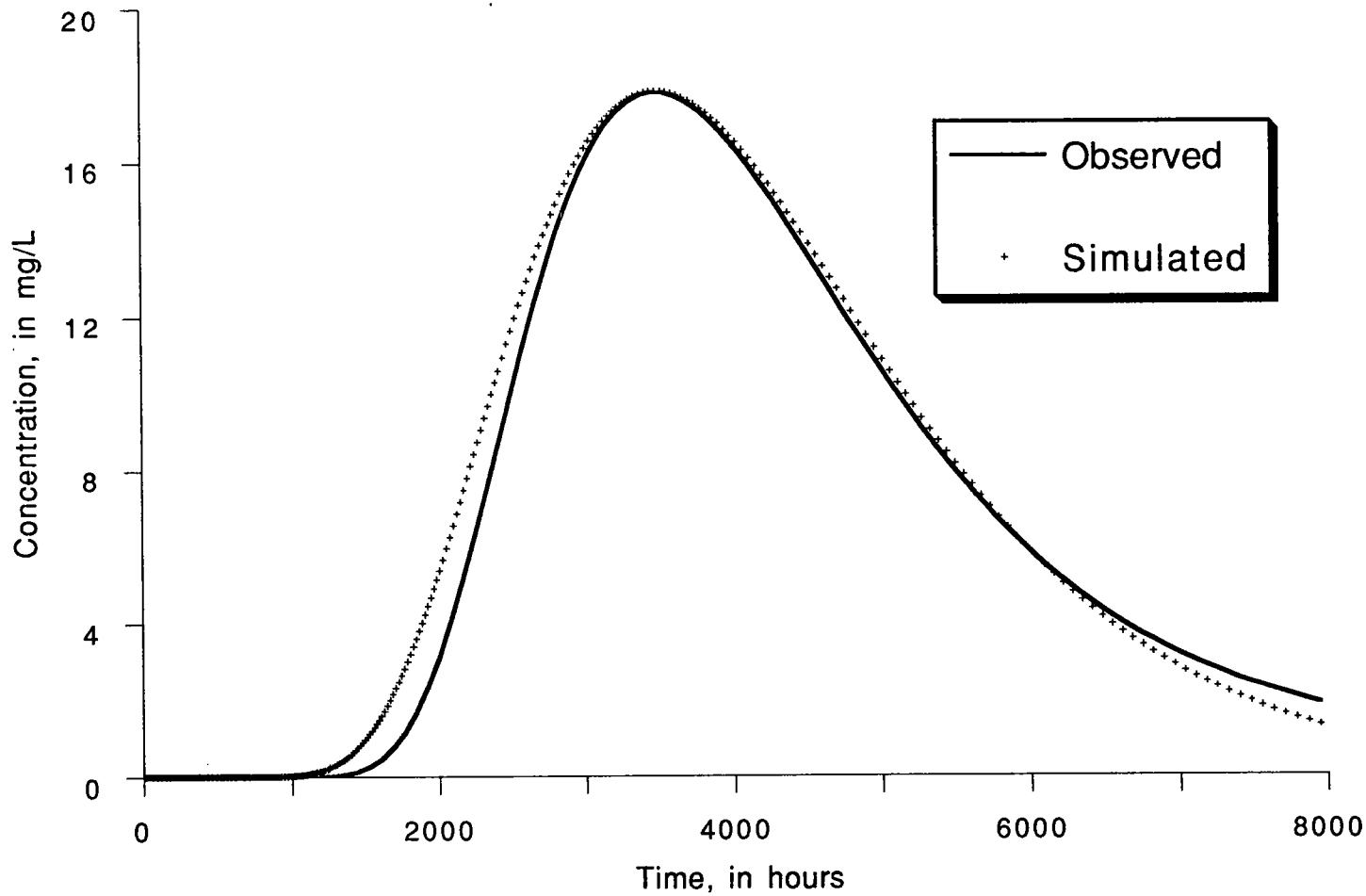

Figure 5. Simulated and measured tracer concentration histories at the down gradient well during the tracer test.

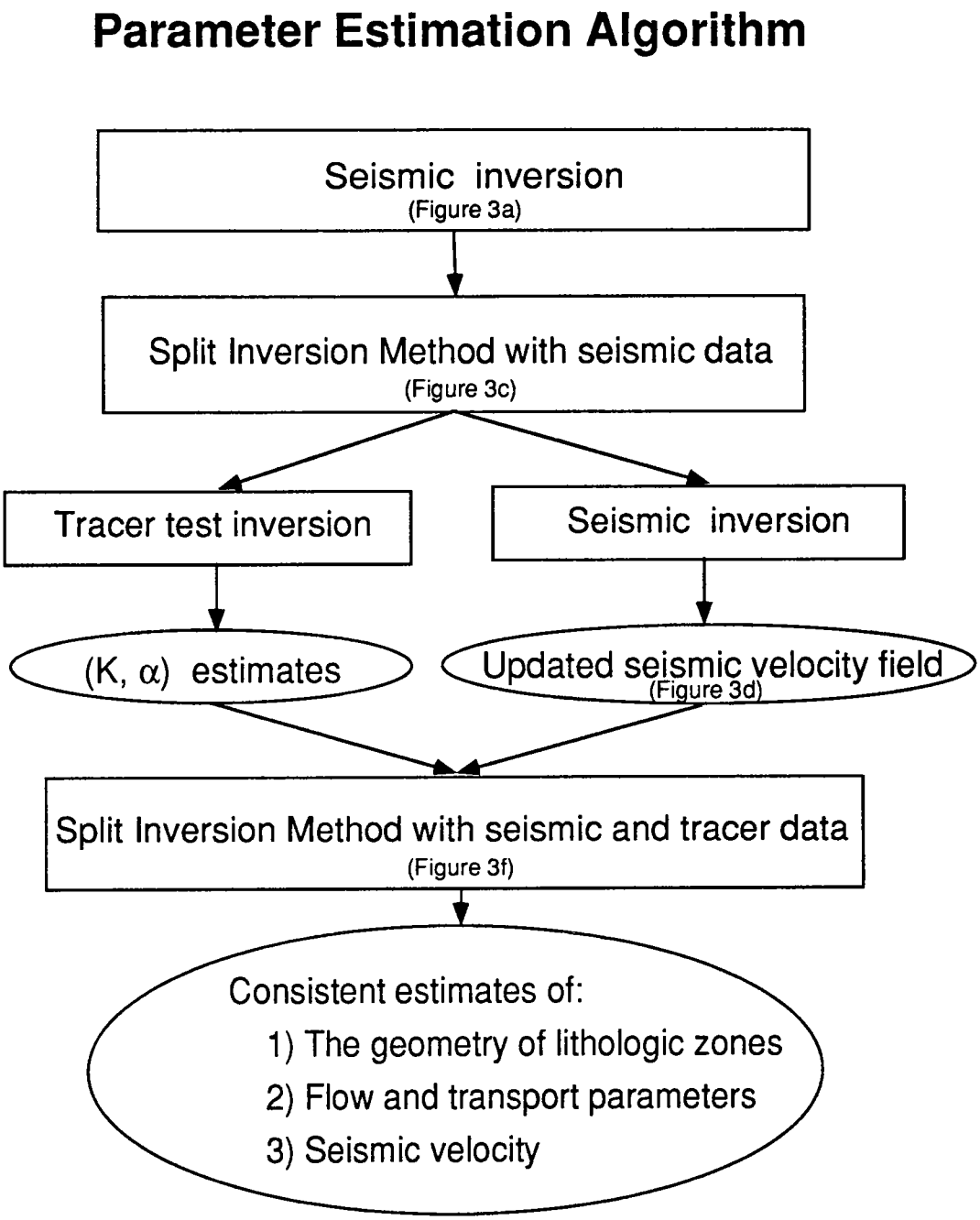

Figure 6. Flow chart of the parameter estimation algorithm. If the estimated lithologic boundaries are not consistent, the routine iteratively updates the boundaries and the parameter estimates. The figure numbers correspond to the tomograms at various stages of the routine

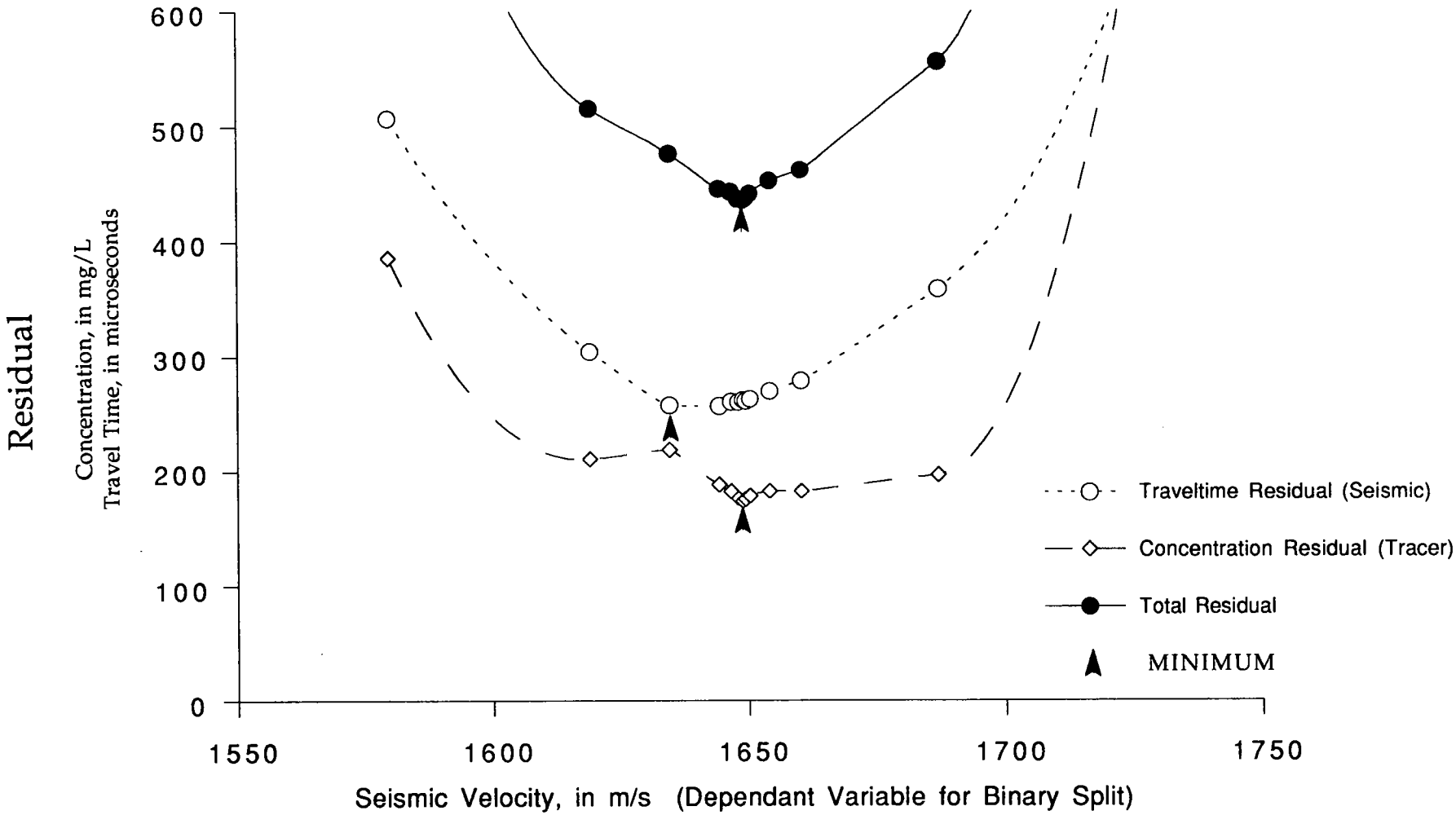

Figure 7. Residuals shown for values of seismic velocity which delineate the lithologic boundaries between sand and clay. The sum of seismic and hydrologic residuals is minimized.